Modeling Sediment and Wood Storage and Dynamics in Small Mountainous Watersheds

Stephen T. Lancaster and Shannon K. Hayes

Department of Geosciences, Oregon State University, Corvallis, Oregon

Gordon E. Grant

USDA Forest Service, Pacific Northwest Research Station, Corvallis, Oregon

We examine controls on supply and transport of sediment and wood in a small (approximately two square kilometers) basin in the Oregon Coast Range, typical of streams at the interface between episodic sediment and wood delivery by mass movements and frequent fluvial sediment transport. We hypothesize that wood deposited by mass movements forms dams that lead to persistent sediment storage and inhibit coherent propagation of sediment pulses. Field data show that much sediment is stored behind such dams and in terraces after the dams breach. We developed a drainage basin-scale model driven by stochastic storm and fire sequences that combines empirical, stochastic and physical models of forest growth, tree fall, wood decay, soil production and diffusion, landslide initiation, debris flow runout, and fluvial sediment transport. In a 3000-year simulation of the study area, woody debris flow deposits form dams on the main channel and lead to steps in the channel profile and terraces on the valley floor that persist in place even after nearly all deposited wood has decayed. Simulated sediment output from the network is relatively steady and shows little evidence of episodic input. Our results suggest that abundant wood plays a key role in moderating sediment flux from small basins following debris flow events. Debris flow events coincident with a lack of abundant wood, such as might occur following forest harvest, could lead to more episodic sediment flux to downstream, fish-bearing reaches.

1. INTRODUCTION

The decline of salmonid species in the Pacific Northwest has prompted increased attention to the temporal and spatial dynamics of aquatic habitat. In particular, various aspects of salmonid life history are influenced by the abundance, location, quality, and spatial distribution of gravel and wood, which create key fluvial environments used for spawning and rearing [*Reeves et al*., 1998]. Although it is widely viewed that hillslope and channel processes influencing erosion, input, transport, or deposition of sediment and wood are inextricably linked to the quality and quantity of aquatic habitat, the degree of coupling in time and space between hillslopes and channels remains a fundamental problem. Specifically, it has proven difficult to show when accelerated mass wasting will occur, how sediment and wood introduced into steep, low-order channels will be routed downstream, and what the long-term consequences of these processes might be for channel and valley floor

Geomorphic Processes and Riverine Habitat
Water Science and Application Volume 4, pages 85-102

morphology, sediment flux, or the quality or quantity of aquatic habitat.

This study addresses sediment and wood dynamics in small (~2 km^2) drainage basins because this part of the landscape represents the interface between mass movements originating on the hillslopes and fluvial transport processes. Woody debris has a potentially strong effect on sediment dynamics and storage in these basins because of the large wood constituent in debris flows and the tendency for wood to form large wood dams [*Kochel et al*., 1987; *Abbe and Montgomery*, 1996; *Montgomery et al*., 1996; *Hogan et al*., 1998; *Massong and Montgomery*, 2000]. Our goal is to better understand how both episodic and chronic inputs of sediment and wood interact with each other and with drainage network structure to produce changing volumes of stored sediment and wood in channels and on valley floors. To that end, we have developed a drainage basin-scale model that encapsulates much of our understanding of the relevant controls on sediment and wood dynamics.

We begin with a review of current approaches to modeling sediment and wood dynamics and distribution in forested mountain streams and then describe our modeling approach. We use the model to simulate sediment and wood influxes to the valley network over millennial timescales, corresponding locations and amounts of sediment and wood storage in the valleys, and sediment outflux from the basin. A comparison of model and field results reveals useful insights into locations, controls, and temporal dynamics of wood and sediment storage and dynamics in upland basins and consequences for interpreting responses of watersheds to disturbance.

1.1. Current Perspectives and Modeling Criteria for Understanding Sediment and Wood Dynamics

Benda and Dunne [1997a, b] used a model to explore the interaction between episodic sediment supply and the channel network in relatively large (~100 km^2) drainage basins. In their modeling they assumed that sediment moves in coherent waves, as documented by *Madej and Ozaki* [1996]. Because of the episodic delivery of sediment from debris flows, the assumption of wave-like translation resulted in the prediction that headwater basins, such as that considered in the present study, are sediment "starved" most of the time.

In contrast, other studies have identified different first-order controls on sediment storage and transport in streams. A function of drainage area and channel slope, a proxy for stream power or sediment transport capacity, discriminated many bedrock and alluvial stream reaches, but only in the absence of wood dams [*Montgomery et al*., 1996]. Sediment supply, lithology, and woody debris have significant effects on the ability to discriminate bedrock from alluvial reaches with a stream power model [*Massong and Montgomery*, 2000]. Some of the factors affecting sediment supply are highly variable in time, such as volumes of sediment-trapping woody debris and recent landslides [*Hogan et al*., 1998]. These studies suggest that, while local sediment volumes may vary over time, they do not necessarily migrate downstream as coherent wave forms but often disperse in place [*Lisle et al*., 1997, 2000].

Existing models to date have only considered sediment stored or transported within the channel proper, and have generally not explicitly included dynamic interactions between wood and sediment. In our experience, in-channel sediment and wood are relatively small fractions of total valley storage, and models to explain long-term evolution of drainage basins should predict storage and dynamics in the valley as well as the channel. More generally, models predicting sediment and wood storage and dynamics in stream and valley networks should account for all processes driving input and output from those networks.

1.2. Study Site: Oregon Coast Range

Field and modeling work were both sited in a 2.1-km^2 tributary to Hoffman Creek in the Oregon Coast Range (Figure 1). We selected the site according to the following criteria: (a) homogeneous lithology; (b) absence of midslope or valley-bottom roads; (c) access to study area; (d) access to land-use records; (e) significant number of recent debris flows; and (f) basin small enough to study and model and large enough to exhibit network-scale effects. The basin is underlain by massive, gently dipping, Eocene Tyee sandstone. The topography is steep—valley sideslopes are typically 40°—and highly dissected with elevations ranging from 10 to 265 m above sea level. Soils are relatively shallow, highly porous, and have low bulk densities (about 1 kg/m^3) [*Reneau and Dietrich*, 1991] (Table 1). The climate is maritime with warm, dry summers and mild, wet winters and mean annual precipitation of approximately 1800 mm [Oregon Climate Service].

The area is forested with primary species Douglas-fir (*Pseudotsuga menziesii*) and secondary species western hemlock (*Tsuga heterophylla*) and western red cedar (*Thuja plicata*) on the hillslopes and red alder (*Alnus rubra*) in riparian areas, though these so-called riparian areas often extend upslope through the smallest hollows to the ridges, especially in immature stands. Nearly half of the basin has been harvested as recently as ca. 1965, and there is field evidence of earlier, undocumented harvest in other parts of the basin. This forest, typical of the Oregon Coast Range,

results in surficial biomass that is less than but of the same order of magnitude as the mass of the soil layer, especially in mature stands, and, therefore, wood is a significant part of the mass moved by landslides and debris flows.

2. MODELING METHODS, ASSUMPTIONS, AND INITIALIZATION

Most of the sediment and much of the wood in streams and valleys originates on the hillslopes. A model encompassing sediment inputs to the valley network must account for sediment production from the parent material, i.e., conversion of bedrock to soil, and delivery of that sediment to the valley via diffusion and mass movements, i.e., landslides and debris flows. Likewise, a model encompassing wood inputs to the valley network must account for biomass growth and delivery to the valley via tree fall and mass movements. Since forest dynamics play a vital role in the timing and location of mass movements, that interaction should be included as well. Some of these processes, such as biomass growth, can be modeled relatively simply (Figure 2). Others, such as debris flows, are more complicated and require more sophisticated modeling.

Our new model is an extension of the Channel-Hillslope Integrated Landscape Development (CHILD) model [*Lancaster*, 1998; *Tucker et al.*, 2001a, b]. As such, the present model operates on a triangulated irregular network (TIN) and shares the CHILD model's drainage area calculation algorithm and stochastic precipitation and runoff generation models.

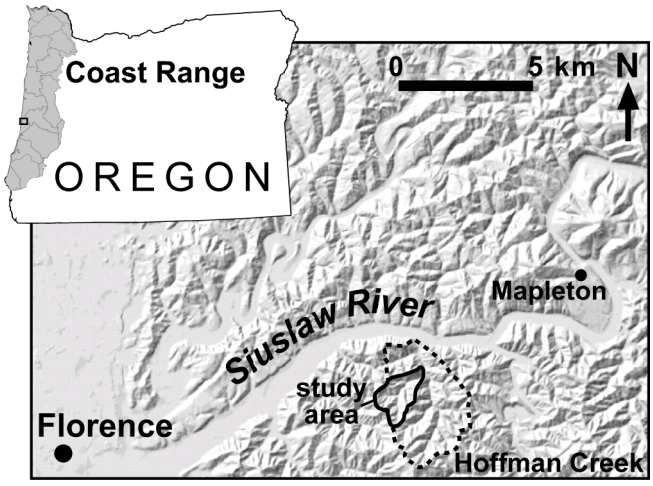

Figure 1. Location map of the Oregon Coast Range showing the Hoffman Creek watershed (outlined with dotted line) and study basin (outlined with solid line).

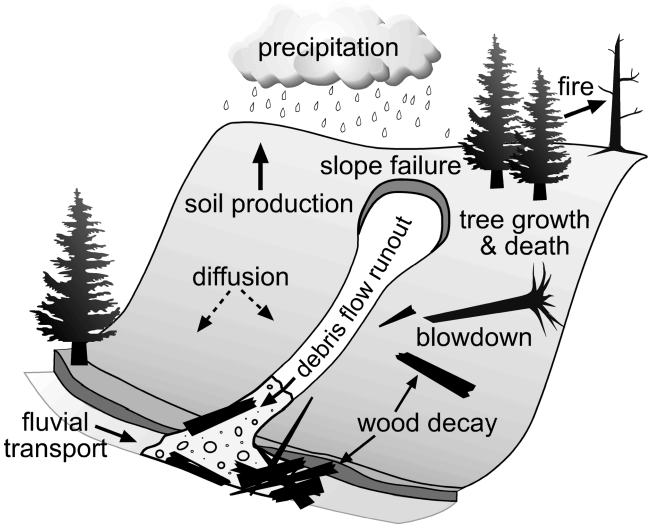

Figure 2. Conceptual figure illustrating the climatic, geomorphic, and vegetative processes simulated in the model.

2.1. Landscape and Storm Characteristics

The model uses gridded digital elevation model (DEM) data with 10-meter discretization to interpolate the elevations of the nodes in the TIN. Node locations are random to eliminate grid bias and form a TIN with the same average discretization as the original DEM. Additional points are added at large drainage areas to eliminate "jaggy" channels typical of interpolated TIN's. Finally, channel-adjacent nodes that would fall within channels are removed [*Lancaster*, 1998]. Nodes in the landscape are classified according to three types: (1) hillslope nodes containing vegetation and soil; (2) channel nodes with wood and sediment deposits and vegetation; and (3) valley nodes with wood and sediment deposits and vegetation (Figure 3). Elevations of hillslope nodes are static because relative elevations on hillslopes do not change much over millennial time scales and any model-driven changes would only decrease the accuracy of topographically driven transport processes [*Dietrich et al.*, 1995]. Channel and valley node elevations evolve over time in response to aggradation and evacuation of sediment and wood because fluvial processes are sensitive to these fluctuations, but bedrock elevations are held static for channel and valley nodes.

We attempt a compromise between the model's descriptiveness and the area modeled by lumping hillslope areas into aggregates. Calculations on each hillslope node (e.g., ~100 m^2) result in a fine-scale map of landscape character-

TABLE 1. Sources and values for landscape, forest, and debris flow parameters

Parameter	Value	Source
Soil storage porosity	0.624	*Reneau and Dietrich*, 1991
Soil flow porosity	0.05	hypothesized
Alluvial porosity	0.40	*Hough*, 1957
Soil cohesion, C_s	500 Pa	*Schroeder and Alto*, 1983
Soil saturated bulk density, ρ_s	1620 kg/m^3	*Reneau and Dietrich*, 1991
Sediment and soil grain density	2660 kg/m^3	*Reneau and Dietrich*, 1991
Soil and alluvial diffusivity	3.2×10^{-3} m^2/yr	*Reneau et al.*, 1989; *Roering et al.*, 1999[a]
Soil production rate for zero soil depth, decay scale	2.8×10^{-4} m/yr, 0.3 m	*Heimsath et al.*, 2001
Soil saturated hydraulic conductivity, K_s	1.0×10^{-3} m/s	calibrated
Alluvial saturated hydraulic conductivity	1.0×10^{-4} m/s	*Montgomery et al.*, 1997
Mean rainfall intensity and duration	1.7 mm/hr, 20 hrs	*Benda and Dunne*, 1997a
Mean interstorm duration	5 days	*Duan*, 1996
Downstream hydraulic width exponent, coefficient	0.5, 7.0 m/(m^3/s)$^{1/2}$	Oregon Coast Range flow vs. width data
At-a-station hydraulic width exponent	0.25	*Leopold and Maddock*, 1953
Downstream hydraulic roughness exponent, coefficient	-0.01, 0.03	*Leopold and Maddock*, 1953
At-a-station hydraulic roughness exponent	-0.21	*Leopold and Maddock*, 1953
Channel drainage area threshold	1.0×10^{4} m^2	field verified
Fluvial transport exponents, m_f, n_f, p_f	0.6, 0.7, 3.0	*Tucker et al.*, 2001b
Fluvial transport coefficient, K_f	1.0×10^{-3} m^{5}s^5/kg^3	hypothesized
Critical shear stress for fluvial transport, τ_c	0	hypothesized
Internal and bed slip friction angles, ϕ_i, ϕ_b	42°, 28°	*Iverson*, 1997
Time step for debris flow motion	0.1 s	calibrated
Deposit erodibility, K_e	1.0×10^{-4} m/s-Pa	hypothesized
Friction factor, C_f	0.02	hypothesized
Critical shear stress for debris flow scour, τ_{cr}	2000 Pa	hypothesized
Maximum root strength	14 kPa	*Burroughs and Thomas*, 1977
Ratio of lateral and vertical root strength, m	2.33	*Burroughs*, 1984; *Hammond et al.*, 1992
Root and biomass growth constants	0.95, 19.05, –0.05	*Sidle*, 1992
Root growth time const.	0.25 yr^{-1}	*Sidle*, 1992
Root decay time constant and exponent	0.5 yr^{-1}, 0.73	*Burroughs and Thomas*, 1977; *Benda and Dunne*, 1997a
Root strength depth constant	2.0 m^{-1}	*Benda and Dunne*, 1997a
Tree height index	40 m	*Means and Sabin*, 1989
Maximum biomass weight	3.00 kPa	*Sidle*, 1992
Biomass time constant	0.12 yr^{-1}	*Sidle*, 1991
Tree diameter at breast height constants, b_0, b_1, and b_2	74.0 m, –0.0105 m^{-1}, 0.911	*Garman et al.*, 1995
Wood decay constant	0.031 yr^{-1}	*Harmon et al.*, 1986
Wood density	450 kg/m^3	
Blowdown parameter	1.0×10^{14} kg/m^3	calibrated
Mean time between fires	200 yr.	*Long et al.*, 1998

a. For reference, *Roering et al.* [1999] obtained the best fit of the linear diffusion model to data with a constant of $5.0\text{x}10^{-3}$ m^2/yr.

istics, e.g., soil depth, vegetation age, and landslide susceptibility. Channel source and channel-adjacent areas form the lumped aggregates (Figure 3b). Nodes are classified and grouped according to the topographic component of landslide susceptibility [*Montgomery and Dietrich*, 1994] such that each aggregate contains several "bins" of nodes with similar susceptibility. During storms each bin, rather than each hillslope node, is considered against a failure criterion using bin-average values of soil depth and root strength. This method saves processing time and mimics the way that

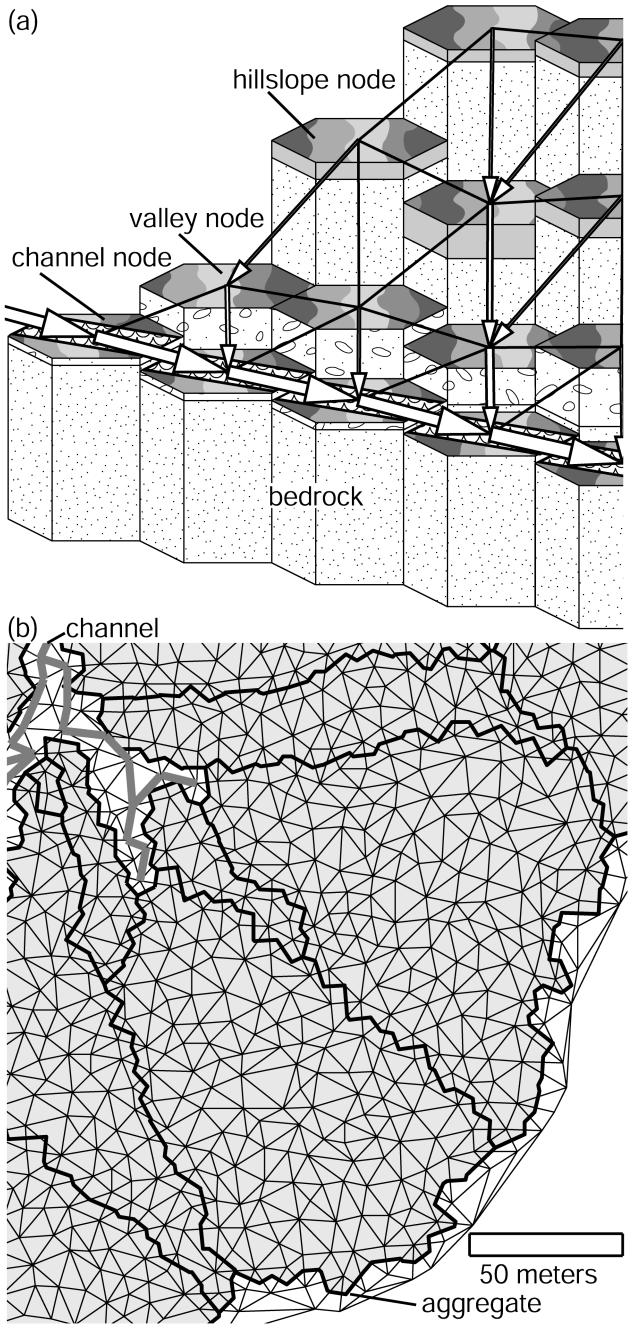

Figure 3. (a) Schematic diagram of nodes, mesh, and flow routing. Nodes are connected by edges of Delaunay triangular mesh and have associated Voronoi areas, i.e., area closer than to any other node. Flow follows steepest edge to neighboring node (arrows). Hillslope nodes have vegetation and soil overlying bedrock; channel and valley nodes have vegetation and alluvium overlying bedrock; and channel nodes contain a channel segment. (b) Part of irregular mesh showing aggregates of hillslope nodes (shaded gray) and channels (thick gray line). Nodes neither within an aggregate nor connected to a channel segment are valley nodes.

whole hollows evacuate during a failure but tends to average out local heterogeneities in soil depth and root strength. The hillslope nodes making up the aggregates are updated upon evacuation of soil and wood during landslides.

The model is fed a stochastic time series of storms based on the work of *Eagleson* [1978], as in *Benda and Dunne* [1997a], *Duan et al.* [1998], *Tucker and Bras* [2000], and *Tucker et al.* [2001b]. The parameters of the stochastic model were derived from storm data for the Oregon Coast Range [*Benda and Dunne*, 1997a] or elsewhere in western Oregon [*Duan et al.*, 1998] (Table 1). In response to each storm event, landslides may initiate and resulting debris flows propagate downstream until they deposit on channel and valley nodes. The storms also drive tree fall. The model records both the runout path and the deposited depths of wood and sediment at each point along the stream. The history of previous events bears directly on later ones: sliding hollows are evacuated of soil, runout paths are scoured of wood and sediment or have wood and sediment deposited, and subsequent debris flows and fluvial transport encounter previous deposits, which may change channel and valley gradients and act as barriers.

The sediment deposited in the valley network by debris flows must originate as hillslope soil, defined here as material lacking the structure of underlying bedrock. Soil depths on hillslopes are governed by soil production and diffusion, where the soil production rate at a point decreases exponentially with the soil depth [*Heimsath et al.*, 1997, 2001]. Diffusion [*Reneau et al.*, 1989; *Roering et al.*, 1999] and soil production [*Heimsath et al.*, 2001] parameter values have been measured in the Oregon Coast Range (Table 1). Though hillslope elevations do not change, soil depths evolve over time. Soil production is only active on the hillslopes, but diffusion acts on all landscape nodes and, thus, may transport material among hillslope, valley and channel nodes. Diffusion of material from a node is contingent on supply—bedrock does not diffuse. The maximum time steps for soil production and diffusion are the storm and inter-storm durations but may be dynamically shortened if necessary for numerical stability [*Tucker et al.*, 2001b].

Channel nodes are those with a drainage area exceeding a threshold of 10^4 m^2, determined from analysis of slope-area plots [*Tarboton et al.*, 1991; *Ijjasz-Vasquez and Bras*, 1995] and trial and error. Channel source area values from field measurements [*Montgomery and Dietrich*, 1988, 1992] produce a channel network with "feathered" extremities on relatively coarse DEMs such as ours. Through field reconnaissance we found that this threshold may exclude some small channels but effectively marks the transition from bowl-shaped hollows to V-shaped valleys. Drainage area is determined by routing each node's area downstream

in the direction of steepest descent. As debris flows deposit sediment and wood and those deposits are re-worked by subsequent debris flows and fluvial processes, the location of the channel may change. When that happens, hillslope and valley nodes may become channel nodes, and abandoned channel nodes become valley nodes.

Sediment deposited in the channel network is transported according to a power law of excess shear stress, where shear stress is represented as a power law of unit discharge and slope derived from continuity and the Manning equation:

$$Q_s \le K_f b\left[\rho g\left(\frac{Qn}{b}\right)^{m_f} S^{n_f} - \tau_c\right]^{p_f} \quad (1)$$

where Q_s is potential sediment discharge, i.e., contingent on supply; K_f, m_f, n_f, and p_f are constants; b is hydraulic width; Q is water discharge; n is Manning's hydraulic roughness; S is hydraulic slope; ρ is water density; g is gravitational acceleration; and τ_c is critical shear stress [*Tucker et al.*, 2001b] (Table 1). Discharge is generated by saturation overland flow, such that alluvial depth in the channel affects discharge, and hydraulic width and roughness are calculated from empirical power laws of discharge, both downstream and at-a-station [Tucker *et al.*, 2001b] (Table 1). Equation (1) represents total load, i.e., both suspended and bed load, for values of p_f in the range of 2.5-3 [*Engelund and Hansen*, 1972; *Vanoni*, 1975; *Govers*, 1992]. This transport law has not been calibrated for streams in the Oregon Coast Range. Rather, it is simple and generic. The most salient feature of equation (1) for the present study is the dependence on local hydraulic slope, which changes during the simulation as a result of sediment and wood aggradation and scour. Our observations indicate that the streams in the study area are not competent to remove wood from debris flow deposits, and these observations are consistent with findings of *Lienkaemper and Swanson* [1987]. Therefore, we assume that wood cannot be transported by fluvial processes, so until they decay, wood deposits act as barriers to sediment transport by decreasing upstream hydraulic slope.

2.2. Landslide Susceptibility

Landslide initiation is stochastic, where the probability of a landslide, i.e., sites that fail and become debris flows, exists when rainfall exceeds a duration-dependent intensity. Our formulation of this critical precipitation is based on *Montgomery and Dietrich* [1994] and *Dietrich et al.* [1995] and lies somewhere between the two in complexity, similar to *Montgomery et al.* [2000]. We assume uniform saturated hydraulic conductivity within the soil layer and zero conductivity beneath that layer. The critical precipitation, P_{cr}, is given by

$$P_{cr} = \frac{K_s h b \cos\theta \sin\theta \rho_s}{A_{eff}\rho_w}\left[1 - \frac{1}{\tan\phi_i}\left(\tan\theta - \frac{C_r + C_s}{h\rho_s g \cos^2\theta}\right)\right] \quad (2)$$

where K_s is saturated soil hydraulic conductivity; h is vertical soil thickness; b is flow width; θ is slope angle; ρ_s is soil saturated bulk density; ρ_w is water density; A_{eff} is effective area contributing to flow and is dependent on storm duration; ϕ_i is internal friction angle; C_r is cohesive root strength; and C_s is soil cohesion (Table 1). We derived a simple expression for the effective area contributing to flow, A_{eff}, by solving the Darcy equation for an effective upslope length contributing to subsurface flow during a storm of known duration, t_d, and squaring that length to get A_{eff}:

$$A_{eff} = min\left[\left(\frac{t_d K_s \sin\theta}{n_{eff}}\right)^2, A\right] \quad (3)$$

where A is topographically defined contributing area; and n_{eff} is the effective porosity for subsurface flow, which field experiments have shown is much smaller than the actual porosity (i.e., the actual travel time is much smaller than that calculated from the actual porosity [*Iverson et al.*, 1997; *Montgomery et al.*, 1997]), most likely because the experiments are actually measuring the arrival of a peak in discharge rather than of the water itself. Using A_{eff} accounts for greater saturation during longer storms but does not account for transient pore pressure increases from short, intense rainfall periods during longer storms. These transient increases may be responsible for many natural failures [*Montgomery et al.*, 1997; *Iverson*, 2000]. We made failure stochastic to account for some of the great uncertainty around predicting actual failure at a site. Greater landslide susceptibility corresponds to lower critical precipitation, P_{cr}, and the probability for stochastic failure during a given storm of intensity, P, is given by

$$Prob(failure) = 1 - \frac{P_{cr}}{P}, P \ge P_{cr} \quad (4)$$

$$= 0, P < P_{cr}$$

Note that saturated hydraulic conductivity, K_s, may vary over orders of magnitude between sites and even within rel-

atively small regions in the field, and critical precipitation is directly proportional to this highly variable and uncertain parameter [*Duan*, 1996]. If this parameter is too small (or too large), failures will occur too often (or too seldom). Because the amount of sediment delivered to the channel network by debris flows is ultimately limited by the soil production rate, K_s will mainly affect soil depths by allowing, or not, realistic amounts of soil to accumulate before failing. We calibrated, albeit roughly, saturated hydraulic conductivity by running several simulations on a small part of the study area while varying K_s's order of magnitude within the range of reported values [*Montgomery et al.*, 1997] and selecting the value that produced reasonable average soil depths on the hillslopes (~0.5 m) [*Montgomery et al.*, 1997; *Heimsath et al.*, 2001] (Table 1).

2.3. Debris Flow Runout

When landslides occur the sediment and wood from hillslope nodes in the failing bin(s) are delivered to the nearest channel where they continue to move as debris flows. To describe debris flow runout, we use a physically-based debris flow model, summarized here, that is simplified to run within the network scale model. *Iverson* [1997] and *Iverson et al.* [2000] developed a model describing debris flow runout with mixture theory and depth-averaged conservation of mass and momentum in two dimensions. We neglect smaller terms and convective accelerations in the momentum balance and treat debris flow motion as a one-dimensional point process, where that point moves with the front of the flow [R. Iverson, U.S. Geological Survey, personal communication, 1999]. Conservation of momentum in the flow direction is then given by:

$$h\frac{\partial v}{\partial t} + v\frac{\partial h}{\partial t} = -\operatorname{sgn} v\left(hg\cos\theta - \frac{p_b}{\rho_m} + hv^2\frac{\partial\theta}{\partial s}\right)\tan\phi_b + hg\sin\theta \tag{5}$$

where h is slope-normal debris flow depth; v is slope-parallel debris flow velocity; p_b is pore pressure at the bed; ρ_m is debris flow mixture density; s is the slope-parallel direction; ϕ_b is bed friction angle (Table 1); and the factor, $-\operatorname{sgn} v$, indicates the direction opposite that of the debris flow velocity. The terms on the left-hand side represent changes in flow velocity and depth, respectively. The first group of terms on the right-hand side resists motion and is therefore multiplied by friction slope. The terms within parentheses represent normal forces on the flow: normal gravitational force, basal pore pressure, and centripetal acceleration due to changes in slope angle, respectively. To get the basal pore pressure in equation (5), hydrostatic pressure is multiplied by 1.8, consistent with the experimental observations of *Iverson et al.* [2000]. The last term on the right-hand side represents the slope-parallel component of the gravitational force.

Debris flow velocity conforms to changes in flow direction, i.e., $v_{new} = v_{old}\cos\alpha$, where α is the angle between the new and old downstream directions. This angle, α, is calculated over a spacing of several nodes (>30 m) both up- and downstream. Debris flow length is held constant. Depth must conform to changes in flow width, i.e., $h_{new} = h_{old}(b_{old}/b_{new})$. Width can cover as many as three nodes and is determined by the flow depth and local channel or topographic geometry. When width and, therefore, depth change, velocity changes as if no forces were acting on the flow, i.e., equation (5) is solved for the change in velocity with the right-hand side set to zero.

Iverson [1997] and *Iverson et al.* [2000] assumed constant debris volume with time. But, we need to model the effects on runout of increases in debris flow volume during runout—*May* [1998] found that on the order of half of debris flow deposit volumes that she measured in the Oregon Coast Range were from entrainment during runout. To model depth changes through scour, we employ a shear-excess law similar to equation (1) with p_f equal to 1, as scour has often been considered to be proportional to shear stress (e.g., *Howard and Kerby* [1983]):

$$\left.\frac{\partial h}{\partial t}\right|_e = K_e(\rho_m C_f v^2 - \tau_{cr}) \tag{6}$$

where K_e is deposit erodibility; C_f is a friction factor; τ_{cr} is critical shear stress (Table 1); t is time; and the rate of scour is constrained to be positive or zero. We assume that bedrock is not erodible. Although the physics of scour by debris flows are poorly understood and equation (6) and its parameters are essentially a hypothesis for that physics, momentum conservation and bedrock's non-erodibility enforce rigorous physical bounds on scour.

Debris flows are processed sequentially with a separate time step (Table 1) and travel from node to node in the direction of steepest descent. Initial width depends on mesh discretization and is approximately 9 m in the simulation presented here, and length is defined by the number of nodes contributing to the initiating landslide. Debris flows are divided into two parts, head and tail, and equations (5) and (6) and the other rules are applied at the head. Head length is total length divided by the number of nodes contributing to the landslide. Scoured and incorporated material is added to the head, and when it stops the front of the tail becomes the new head with the old head's prior velocity. This scheme accounts for two observations. First, scoured material and accumulated debris usually remain at

the front. Second, tails often bypass the more debris-laden heads when the latter stop. Our scheme retains a feasible simplicity while allowing process dynamics to determine the final deposit geometry.

Unlike any other debris flow runout model that we are aware of, ours incorporates all three major constituents observed in the field: sediment, water, and wood. Debris flows must incorporate all surface wood in their paths or stop. As with sediment, we use equation (6) to model scour of wood from deposits. We neglect any other effects of wood, such as the resistance by standing trees to uprooting or breakage and any extra resistance due to the shape and strength of the wood pieces, because a previous series of model experiments determined that the simulated runout length distribution was closest to an observed distribution without these other effects.

2.4. Forest Growth, Root Strength, Blowdown, and Wood Decay

As indicated above, the presence of wood in channels affects fluvial sediment transport; the strength of tree roots affects landslide susceptibility; and the presence of wood on hillslopes and in valleys affects debris flow momentum. Therefore, we must account for these effects by modeling: (a) growth and decay of tree roots; (b) growth and decay of wood biomass; (c) stochastic movement of wood, e.g., from riparian areas to channels, by treefall; and (d) stochastic events resulting in forest death, i.e., fires.

The evolution of several variables describing the forest is governed by a set of empirical equations, the parameters of which vary according to species. We have chosen parameter values that are representative of Douglas-fir (*Pseudotsuga menziesii*) because it is the dominant species in the field area. Root strength, C_r, evolves according to exponential decay of root strength after stand death and sigmoid-increasing strength, as in *Sidle* [1992] and *Duan* [1996], and partitioning of root strength between vertical and lateral components, with the vertical component decreasing exponentially with soil depth. Some parameter values used in root strength calculation were derived specifically for the Oregon Coast Range, while others are generic (Table 1). The lateral and vertical components of root strength are summed to get the total root cohesion, C_r, which is added to soil cohesion in equation (2). In our model, root strength can decay from an arbitrary value rather than being constrained to decay from the maximum value. Also, we use a differential form so that root strength at the next time step evolves from the present value. Upon stand death, the constants representing "initial" lateral and vertical root strength, C_{V_0} and C_{L_0}, respectively, are reset from the total root strength at the time of death, C_{r_0}, according to a partitioning coefficient, m:

$$C_{V_0} = \frac{C_{r_0}}{1+m},\ C_{L_0} = mC_{V_0}. \tag{7}$$

This root strength model neglects scale effects. In reality, larger failure perimeters should have larger lateral root strength [*Montgomery et al.*, 2000], but, in practice, the model does not calculate failure perimeter.

Wood volume grows as the stand ages according to the sigmoid function of *Sidle* [1992]. Again, our model employs a differential form during evolution so that biomass at the next time step evolves from the present value. Parameter values for this relationship are generic (Table 1). Maximum tree height is determined by *Richards*'s [1959] equation on a 5-parameter base as used by *Duan* [1996] and evolves with time according to a differential form of that equation. The tree height index used in the maximum tree height relationship was derived for Douglas-fir in the Oregon Coast Range [*Means and Sabin*, 1989] (Table 1).

Tree diameter at breast height (D_{bh}, height = 1.37m) is calculated by inverting an empirical relationship describing height as a function of D_{bh} [*Garman et al.*, 1995] to solve for it as a function of maximum tree height, H_w:

$$D_{bh} = \frac{1}{b_1}\ln\left[1-\left(\frac{H_w - H_b}{b_0}\right)^{\frac{1}{b_2}}\right],\ H_b < H_w \le b_0 \tag{8}$$

$$= 0,\ H_w \le H_b$$

where b_0, b_1, and b_2 are empirical coefficients determined for Douglas-fir in the Oregon Coast Range [*Garman et al.*, 1995], and H_b is breast height, 1.37 m. In order that the argument of the logarithm does not become negative, tree height may not exceed b_0.

Trees fall via a stochastic blowdown model. The number of trees falling at a given landscape node during each storm is exponentially distributed, and the mean, or expected, number of blowdowns, μ_N, is given by the ratio of the drag force from wind to the resisting strength of roots:

$$\mu_N = \frac{P^2}{C_r}\left(\frac{\rho_a C_d V_R^2}{2B_T}\right) \tag{9}$$

where P is the storm precipitation rate; C_r is the root strength; ρ_a is the density of air; C_d is the drag coefficient; V_R is the ratio of storm wind velocity to precipitation rate; B_T is the ratio of tree crown width (i.e., the cross-sectional

area presented to the wind divided by tree height) to height. Shelter or exposure effects are neglected. The term in parentheses is lumped into a single "blowdown" parameter for model input (Table 1). The order of magnitude of this parameter is calibrated to provide slightly decreasing live biomass over time for old-growth stands, as has been observed in the Oregon Coast Range [T. Spies, U.S. Forest Service, pers. comm., 2000]. As in *Van Sickle and Gregory* [1990] and *Robison and Beschta* [1990], fall direction for each blowdown is chosen at random. Wood is distributed over the nodes on which the tree falls as if it were a perfect cone with the maximum tree height and D_{bh} calculated from equation (8), and biomass is conserved, i.e., a tree cannot fall from a node unless it has enough live biomass. In this way, wood is contributed to the channel from riparian zones and, depending on the tree height, may come from several nodes' distance. Fallen and deposited wood decay over time according to a single exponential [*Harmon et al.*, 1986] with a rate derived for Douglas-fir in western Oregon (Table 1).

Fires occur at exponentially distributed intervals and kill the entire forest, whereupon all trees fall. In nature, fires have variable size and intensity, and many trees are left standing, but, for simplicity, we assume we may neglect these variations. Neglecting size variation is justified by the finding that nearly all fires are larger than the basins we model (i.e., < 5 km^2) [*Wimberly et al*., 2000; M. Wimberly, U.S. Forest Service, pers. comm., 2000]. As stand-killing fires typically burn only a small fraction of existing biomass [*Huff*, 1984; *Harmon et al.*, 1986; *Spies et al.*, 1988], we assume that fires consume no wood.

2.5. Model initial conditions from digital elevation models and surveyed channel profiles

The initial topography for the model simulations was generated from a 10-meter digital elevation model (DEM) and characteristics of the longitudinal channel profile. The DEM was generated from 7.5 minute topographic maps. For the purposes of modeling locations of sediment storage, the DEM-based valley topography is inappropriate because it results in a longitudinal channel profile with large steps and intervening "flats" as long as several hundred meters such that sediment accumulates on the flats. The problem is exacerbated by the fact that the model considers this initial profile to be bedrock and, therefore, not erodible. To remedy this problem we used characteristics of the longitudinal channel profile surveyed in the field to make a smooth initial bedrock profile.

It is often observed that stream gradient, or slope, and contributing area are related as,

$$S = KA^{-\theta} \tag{10}$$

where θ is the concavity index; and K is the steepness index [*Flint*, 1974]. This relationship has been used in many studies to characterize streams [e.g., *Hack*, 1957; *Tarboton et al.*, 1991; *Willgoose*, 1994; *Moglen and Bras*, 1995; *Tucker and Bras*, 1998]. By finding contributing areas with the DEM and matching the longitudinal profiles from the DEM and field survey, we found the contributing area at every point along the surveyed profile. We then used the surveyed profile and the DEM contributing areas to derive K and θ (Table 2). We used the method of *Snyder et al.* [2000], in which the slopes are calculated between 10-meter elevation intervals from the surveyed profile. To extrapolate a bedrock surface from the outlet up every branch of the network with equation (10), we "tuned" the steepness and concavity indexes to transition smoothly with the DEM elevations along the main channel (Table 2). This method resulted in steps along some tributary channels, but these steps are unlikely to affect the results for the main channel.

In order to avoid an entrenched bedrock profile only one node wide, we repeatedly determined drainage directions according to a probabilistic criterion such that the probability of flowing to any downslope neighbor is proportional to the relative magnitude of the slope in that neighbor's direction (whereas at all other times in the simulation flow direction is deterministic and follows steepest descent). The bedrock elevation was calculated for every channel node each time flow directions were re-determined, but node elevations were not changed until the end, when elevations at all nodes that had been channels, i.e., channel and valley nodes, were changed. This method resulted in some elevated bedrock "terraces" with thick soil adjacent to the channel, especially in the lower reaches of the main channel (Plate 1a). The profile-smoothing procedure successfully eliminated the main channel steps and flats that were artifacts of the DEM.

Finally, we developed a procedure to provide both heterogeneous soil depths in landslide-prone hollows and realistic soil depths on ridges and side-slopes. An initial soil layer evolved by diffusion and soil production over 6000 years (as in, e.g., *Dietrich et al.*, [1995]). The storm model ran in isolation for 100 years to find the maximum intensity and duration during that time. Assuming a 6-year-old forest, when root strength is at a minimum, we determined failure areas given a storm with that intensity and duration, and the soil was removed from these areas. At this point, most of the landslide-prone hollows were emptied of soil, but soil remained on the ridges and planar slopes. In order to refill the hollows to different depths to mimic different

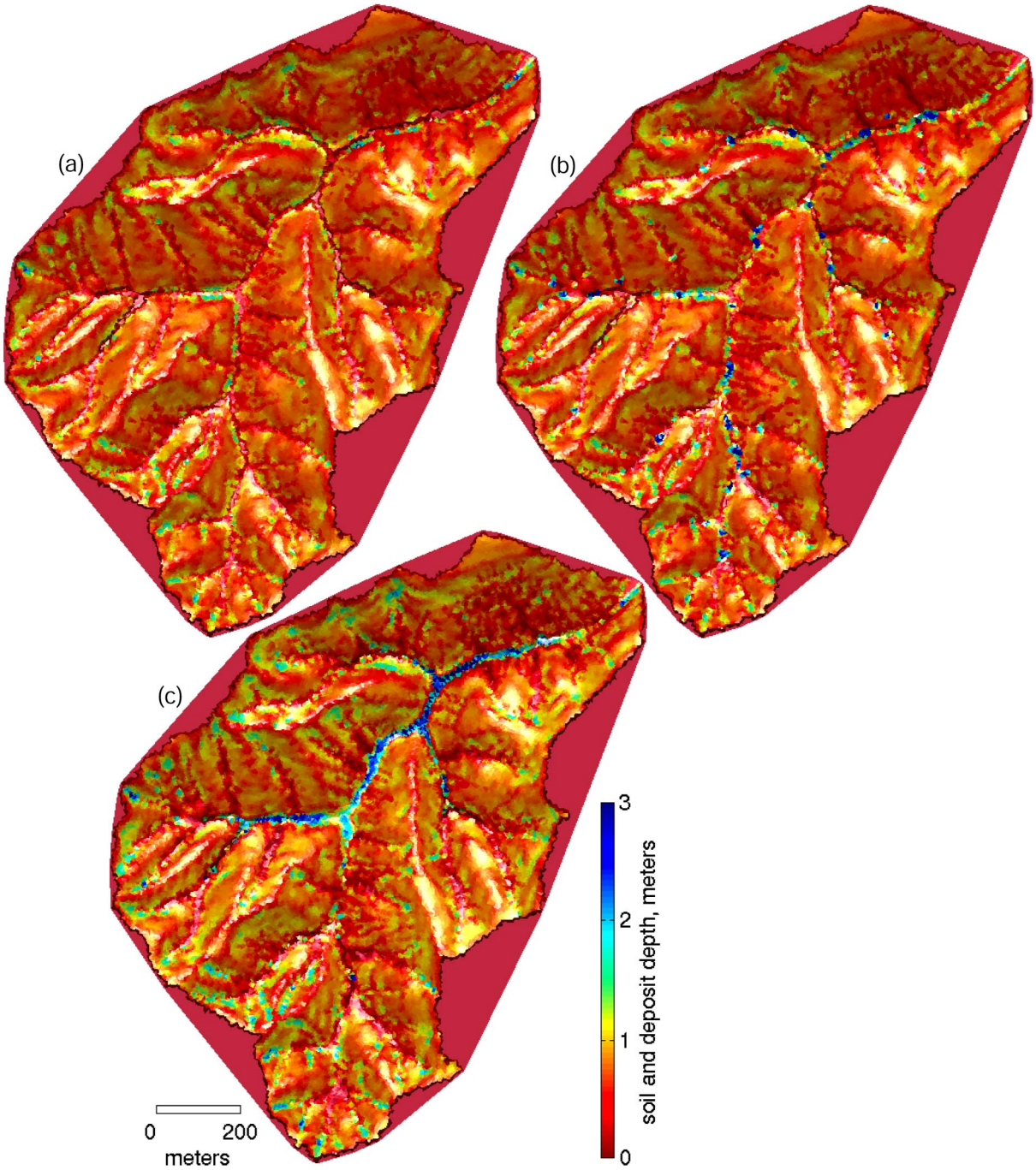

Plate 1. Shaded relief maps colored according to soil or sediment depth of (a) initial condition for model simulation, (b) after 200 years (18 years after the first fire), and (c) after 3000 years (the end of the simulation). The color scale is compressed to show variations in soil depth and to highlight all deposits greater than 3 meters in depth.

TABLE 2. Parameters of slope-area relationship, both derived from data and "tuned"

Range of contributing area, A (m^2), used for derivation	Range of contributing area, A (m^2), to which tuned profile was applied	Derived concavity index, θ	Tuned concavity index, θ	Derived steepness index, K	Tuned steepness index, K
$10^5 \le A < 10^6$	$8.5\times10^4 \le A < 10^6$	0.407	0.41	14.8	13.5
$A \ge 10^6$	$A \ge 10^6$	1.41	1.41	1.63×10^7	1.6×10^7

times since failure, evolution of the soil layer then proceeded for different random times between 0 and 2000 years in each aggregate. The forest at each failure site was regrown for the lesser of 300 years or the randomly chosen time of soil evolution to provide an old forest on all nodes except those that had recently failed. Finally, the landscape evolved for 10 more years while it was submitted to stochastic storm input, and during this time failed soil was removed from the system. This procedure produced a heterogeneous, realistic initial soil layer (Plate 1a) and prevented a massive initial influx of debris flows to the valley network.

3. PREDICTING SEDIMENT AND WOOD FLUXES

3.1. Simulation and Field Methods

Beginning with the initial condition described in the previous section, we simulated a period of 3000 yrs. in the study basin (Plate 1). In order to adequately represent the spatial distribution of sediment and wood inputs to the valley network, the model must adequately represent observed runout lengths.

In order to locate all recent debris flows in the study basin, we attempted to walk the entire channel network defined by a 10^4 m^2-contributing area threshold. We identified 35 debris flow deposits, and were able to measure the runout length from source area to deposit for 28 of them. Horizontal runout length was then measured between failure source and deposit terminus on a DEM using a GIS. We grouped all measured debris flows into approximate age classes based on aerial photographs (1945-1997) and the age of trees growing on the deposits. We also measured total deposit and wood constituent volumes and down wood volumes in several of the smaller channels [*Harmon et al.*, 1986]. Although we tried to capture the full failure history of the study basin, evidence of many smaller events is erased over time as new failures occur, and therefore the older part of our record is skewed towards large events.

3.2. Simulation Results and Comparison to Field Data

We test how reasonable the modeled sediment and wood fluxes are by comparing simulation results to field data. We check modeled debris flow runout length, size, sediment and wood input rates, and longer term denudation rates. Our main concern is correctly simulating the spatial distribution of sediment input to the channel network from debris flows.

The cumulative distribution function (CDF) of simulated debris flows mimics the CDF of the 28 debris flow runout lengths measured in the study basin (Figure 4). The spatial distribution of debris flow inputs to the valley network is therefore reasonably accurate.

Simulated debris flow sizes are also similar to measured failure volumes. The average debris flow volume for the simulation is 165 m^3, well within the range of reported values (Table 3). Our own field measurements of wood in debris flow deposits also indicate that wood volumes predicted by the model are reasonable.

The simulated failure rate per unit area is similar to the measured rate in the study area. From 35 debris flows in the study area within the last 50 years, we calculate a failure rate of 0.33 km^{-2} yr^{-1}. Since the mean fire recurrence interval for this area is approximately 200 yrs [*Long et al.*, 1998], or one basin-wide disturbance in 200 years, and nearly half the basin was clearcut in 50 years, approximately equivalent to one basin-wide disturbance in 100 years, the measured debris flow rate may exceed the long-term "natural" rate by a factor of about 2 such that the "correct" rate is closer to 0.17 km^{-2} yr^{-1}. During the 3000-year simulation, 1182 debris flows occurred, for a failure rate of 0.191 km^{-2} yr^{-1}, which is similar to the estimated natural rate for the study area. This value is low compared to short-term landslide frequencies reported in the literature (Table 3), but higher than the long-term failure rate, based on measured lowering rates, of 0.01–0.03 km^{-2} yr^{-1} calculated by Montgomery *et al.* [2000].

Other comparisons suggest that the rate and timing of landslides may not be realistic. Extended periods of several hundred years pass in the simulation without a landslide event, and the time series of simulated debris flow events shows that, except before the first fire, all debris flows occur shortly after fires (Figure 5a). *Schmidt et al.* [2001] found that landslides in older forests occurred in significant gaps between trees. The model's binning procedure averages out such heterogeneities in root strength and makes failures in older forests unlikely. Soil storage increases dur-

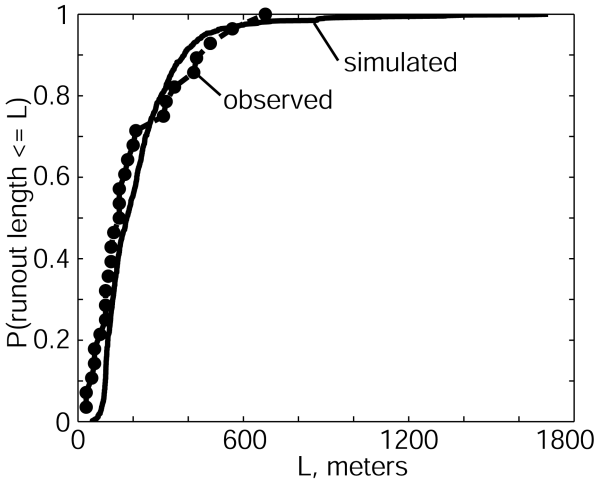

Figure 4. Simulated and observed cumulative distribution functions of debris flow runout length, i.e., sample probability of runout length less than or equal to some length, L.

ing the simulation (Figure 5b), and the simulated denudation rate from landslides, 0.0158 mm yr^{-1}, is low relative to the bedrock lowering rate determined from colluvial transport of 0.061 ± 0.025 mm yr^{-1} [*Reneau and Dietrich*, 1991] and from soil production of 0.1 mm yr^{-1} [*Heimsath et al.*, 2001]. The coarseness of the DEM-derived topography should lower effective diffusion rates below those observed in the field, and errors in hillslope gradient will affect landslide susceptibility. Both of these factors could lower the denudation rate from landslides. Neither of these possible shortcomings affect the spatial distribution of sediment input by debris flows.

In contrast to the event-based sediment input dominated by debris flow deposition (Figure 5b), simulated sediment output from the basin is relatively smooth because it is controlled primarily by fluvial transport (Figure 5c). Occasional debris flows reaching the outlet lead to small steps in the cumulative output coincident with debris flow occur-

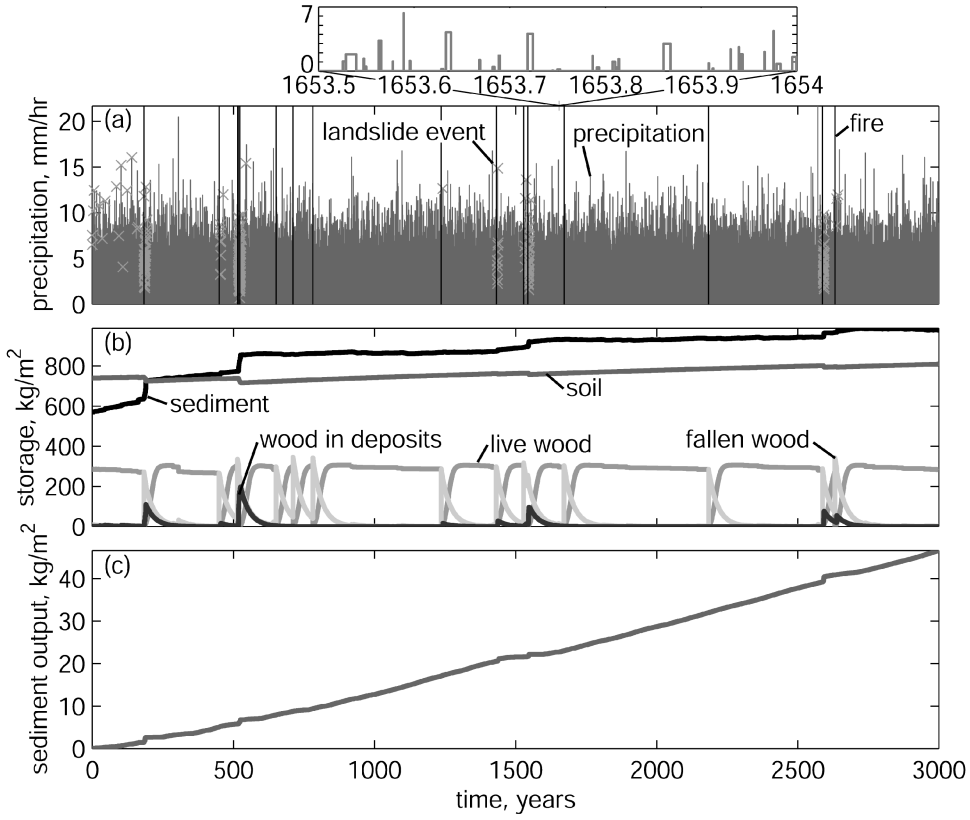

Figure 5. (a) Precipitation intensity *vs.* simulated time, indicating fires and landslide events. Part of the precipitation series (0.5 years) is shown with a dilated time axis to illustrate variations in storm duration and intensity and interstorm periods. (b) Normalized storage masses *vs.* simulated time: sediment and wood in deposits normalized by valley area (sum of channel and valley node areas); soil normalized by hillslope area (sum of hillslope node areas); live wood and fallen (dead) wood (excluding wood in deposits) normalized by basin area (sum of all hillslope, valley and channel node areas). (c) Mass of cumulative sediment output normalized by basin area *vs.* simulated time.

TABLE 3. Summary of the present study and landslide and debris flow studies in areas geologically similar to the Hoffman Creek site in the Oregon Coast Range

Average landslide volume (m^3)	Landslide frequency (km^{-2} yr^{-1})	Number	Period of record (yr)	Reference
610	N/A	73	single storm	*May*, 1998
450	N/A	36	N/A	*Benda and Cundy*, 1990
54	0.533	39	15	*Swanson et al.*, 1977[a]
110	1.03	317	10	*Swanson et al.*, 1977[b]
250	8.0	35	10	*Montgomery et al.*, 2000
	5.8	25	10	*Montgomery et al.*, 2000[c]
20	N/A	92	single storm	*Robison et al.*, 1999[d]
115	N/A	76	single storm	*Robison et al.*, 1999[e]
	0.33	35	50	field data, present study
165	0.191	1182	3000	simulation, present study

a. field-based survey in mature forest
b. air photo-based survey in recent clear-cut
c. non-road-related slides only
d. landslide initiation site only, Mapleton, Oregon, site only
e. landslide and non-channelized debris flow, Mapleton, Oregon, site only

rences, and impoundment of sediment by woody debris causes a relative flattening of sediment output in periods following these occurrences and lasts for approximately 100 years. This period of flattened sediment output is coincident with the period over which wood deposits decay (Figure 5b). The sediment output during the simulation is equivalent to a denudation rate of 7.6 x 10^{-3} mm yr^{-1}, indicating that roughly half of the denudation by debris flows is stored in the valley network at the end of the simulation.

4. PREDICTING LOCATIONS AND AMOUNTS OF SEDIMENT AND WOOD STORAGE

4.1. Simulation and Field Methods

To quantify simulated sediment and wood storage, we calculated the cross-sectional area of simulated deposits at each point along the main channel. The down-valley direction was determined by fitting a line to the channel node and the next three downstream nodes. From the channel node, sediment and wood depths were read, or "measured", at 0.1-meter intervals along line segments perpendicular to the down-valley direction to the right and left as long as the measurement points were still within the valley, i.e., belonged to a channel or valley node, and were within a maximum of 20 meters from the channel node. This latter criterion was based on the maximum valley widths measured in the study area and was necessary to keep the simulated valley transects from extending up tributary valleys. These "surveys" provide snapshots of simulated valley storage at each model output time, every 20 years. We also calculated average storage along the main channel by putting each of the instantaneous measurements into 50-meter bins and calculating the average for each bin.

We determined sediment and wood storage in the field by a similar method. We surveyed the longitudinal profile of the main channel of the study basin with a hand level and stadia rod. This survey was relatively detailed, with usually <5 channel widths between survey points. At longer intervals, ~10 channel widths, we surveyed valley transects. Using the valley transects and the assumption of 40° valley side slopes, we calculated the cross-sectional area of sediment stored above the elevation of the channel. This information combined with the channel survey allowed us to calculate the sediment stored in the valley above the elevation of the channel (Figure 6). Where the channel bed is bedrock, sediment stored above the channel is equal to the sediment stored in the valley. Where valley floor deposits formed distinct wedges, i.e., relatively flat surfaces followed by downward steps, we estimated the cross-sectional area of valley floor storage with a line connecting the beginning of the flat surface to the bottom of the step. Includ-

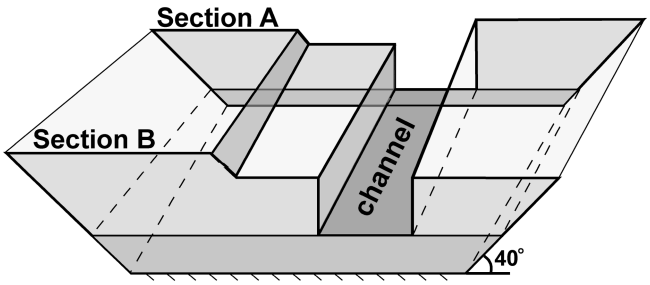

Figure 6. Schematic diagram of the sediment volume estimation method. Storage is calculated for sediment and wood both above the channel bed and including some sediment and wood below the channel bed in distinct wedges detectable from the longitudinal channel profile.

ing these wedges yielded a second, larger estimate of valley storage (Figure 6).

4.2. Simulation Results and Comparison with Field Data

Comparing simulation and field results following a similar disturbance, fire in the case of the simulation and partial clearcutting in the case of the field area, indicates that the model accurately predicts many of the observed sediment and wood accumulation features both in terms of spatial distribution and magnitude (Figures 7, 8a).

Cross-sectional areas of valley floor sediment and wood storage show that local storage maxima are often associated with steps in the longitudinal channel profile (Figure 7). Some storage maxima, however, are not associated with channel steps, e.g., the storage maximum near the bedrock points in the middle of the profile. This fact indicates, and our observations confirm, that much of the storage on the valley floor is in fans and terraces that are incised by the channel.

As sediment and wood influx in our model are dominated by debris flows, the pattern of debris flow deposition dominates the pattern of storage early in the simulation (Plate 1b) and many of the storage peaks are dominated by wood (Figure 8a). These storage peaks are associated with large steps in the longitudinal channel profile, many of which actually form dams (Figures 8a, 9a).

Over 100 years of simulated time, wood deposits decay, and sediment deposits are reworked by fluvial transport (Figures 5b, 8b, 9b). The same peaks are evident at the same locations, and the dams have become steps (Figures 8b, 9b). For example, the location of maximum storage is the same, approximately 600 m downstream, at 200 and 300 years, and at 300 years the channel step associated with this maximum is still pronounced. Dams at 200 years lead to fluvial deposition upstream such that stored sediment volume at some places actually increases between 200 and 300 years. For example, the magnitude of the storage peak at 1200 m downstream decreases slightly between 200 and 300 years, but the wood component decays while the sediment component increases (Figure 8). This increase must be due to fluvial deposition because no debris flows occurred in the interval (Figure 5a).

None of the storage peaks move between 200 and 300 years, and persistent peaks in storage are also evident in the average storage profile (Figure 10). The valley cross-sections in the neighborhood of the location of maximum storage show that at 300 years the channel has incised the deposit and formed a high terrace that accounts for most of the storage in the cross-section (Figure 9). If this cross-section is typical of others, then most of the storage in the valley at 300 years is in terraces, resulting in persistent stationary storage peaks. The actual amount of storage in terraces is influenced by bank erosion or channel avulsion due to local wood input, which will tend to increase terrace erosion. Conversely, lower decay rates for buried wood and decay-resistant species would tend to increase the longevity of dammed deposits. These effects are not represented in the current model.

Toward the end of the simulation, storage is dominated by an area of fluvial deposition in the middle of the lower half of the profile (Figure 10) because the fluvial model created a graded profile to smooth out the difference in concavity between the upper and lower parts of the initial bedrock profile (Table 2). Note that, because the elevation at the basin outlet is fixed, the reach near the outlet cannot aggrade.

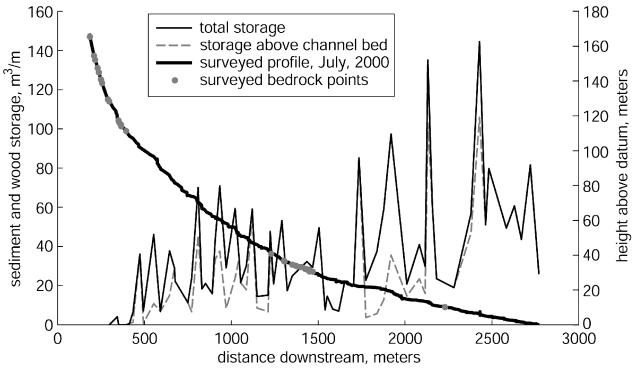

Figure 7. Surveyed Hoffman Creek channel profile with bedrock points highlighted and cross-sectional areas of sediment stored in surveyed valley transects *vs.* distance from divide. Two storage estimates are shown: sediment stored above the channel bed, representing a minimum estimate; and a more realistic estimate including sediment "wedges".

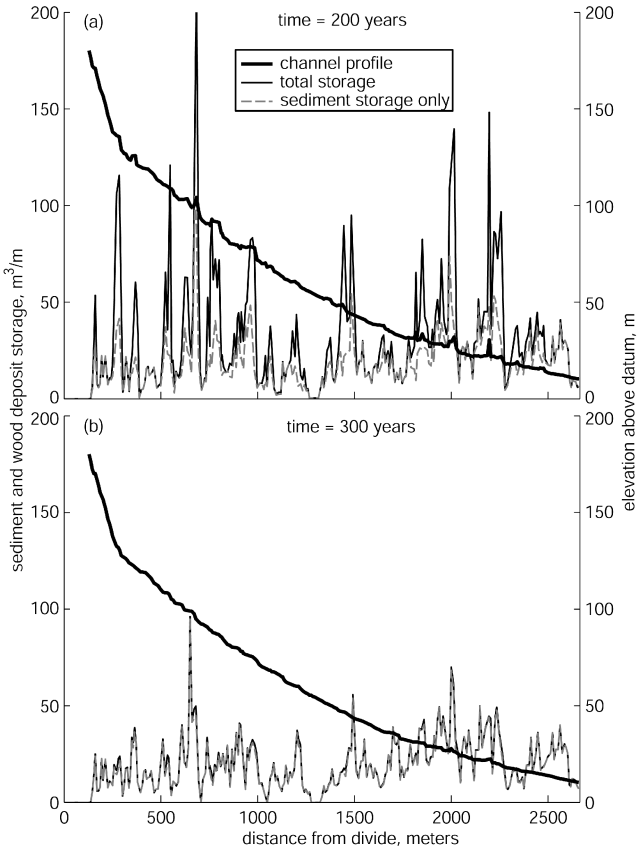

Figure 8. Simulated main channel profile and cross-sectional areas of sediment and wood deposit storage at every point along the main channel *vs.* distance downstream at two times, (a) 200 years (18 years after the first fire) and (b) 300 years (118 years after the first fire and before the second fire).

5. DISCUSSION

In small mountain drainage basins where debris flows are common, such as the study area, large deposits composed of both debris flow and fluvial deposits are the rule rather than the exception, as overlapping parts of the valley network receive debris flows and fluvial deposition from diverse sources. The simulation reproduces this phenomenon.

The model predicts that relatively large quantities of sediment and wood are stored high in the network, in small, headwater streams and their valleys. The amounts of storage predicted by the model are comparable to the volumes observed in the field. This prediction was contingent on reproducing the correct spatial distribution of debris flow inputs to the network, i.e., mimicking the observed distribution of debris flow runout lengths. These large storage volumes predicted by the model are composed of both debris flow and fluvial deposits, similar to what we observe in the field.

The model correctly predicts the existence of nodal points of sediment and wood accumulation, and, in the short term, the relative magnitudes of these storage peaks are close to those of the data (Figures 7, 8a). In the simulation these nodal points of larger storage fluctuate volumetrically but remain stationary and persist over time such that even the average storage has distinct maxima and minima along the profile (Figure 10). Storage nodal points are stationary because deposition leads to more deposition. Even as wood dams decay, impounded sediment is not released all at once. These wood dams lead to depositional zones because deposition behind dams reduces stream gradient and, thus, transport capacity in these zones.

These depositional zones negate the possibility of coherent, wave-like sediment movement. Rather, sediment tends to accumulate at and move between these "sticky spots" in the network that correspond to locations of frequent debris flow deposition, e.g., at changes in valley width and flow direction, both of which often occur at tributary junctions. These deposits can grow over time as they trap sediment

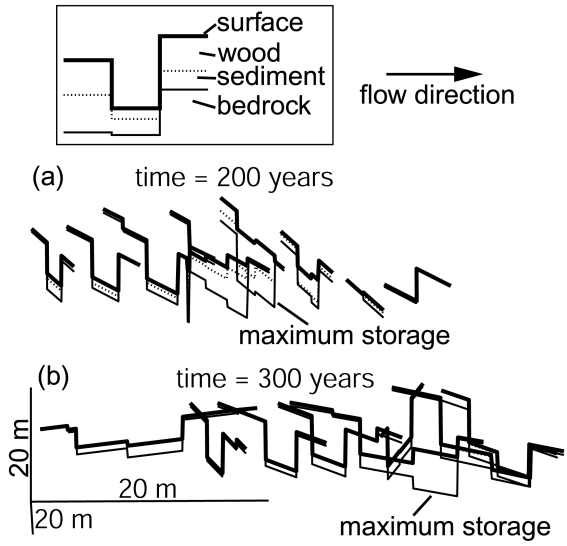

Figure 9. Simulated valley cross sections of the maximum sediment and wood deposit storage at (a) 200 years and (b) 300 years. At the earlier time (a), wood and sediment fill the valley floor and form a dam at the location of maximum storage. Later (b), almost all wood has decayed, but a sediment wedge remains. The channel is incised into the sediment such that most of the sediment at the location of maximum storage is in a terrace next to the channel. Note that the channel takes a different route through this part of the valley between the two times shown.

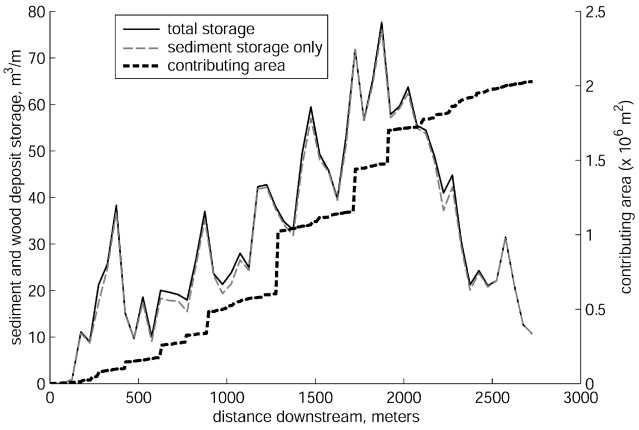

Figure 10. Cross-sectional areas of sediment and wood deposit storage averaged over 50-meter channel segments and samples every 20 years for the 3000 year simulation, and contributing area at 3000 years *vs.* distance downstream. Step-increases in contributing area occur at tributary junctions.

transported from upstream, and shrink as the valley-spanning wood jams that help dam sediment decay.

Small mountain drainage basins, then, add capacitance to the system. The pulsed sediment input to the system does not cause pulsed output, as we might expect if sediment deposits translated as waves, as posited by *Benda and Dunne* [1997b]. Rather, these small basins absorb the sporadic and abrupt inputs of sediment from debris flows and output a relatively smooth fluvial sediment transport signal, as posited by *Massong and Montgomery* [2000]. Management practices that remove wood from the system would likely remove much of this capacitance and dramatically alter the sediment output of small basins to larger, fish-bearing streams.

Complex interactions among sediment, wood, climate, and disturbance regime necessitate use of a complex model, albeit with simple parts, to explore sediment and wood delivery to the channel network, storage patterns, and subsequent transport. We do not presume to test the model as a predictive tool. Rather, the model represents a kind of hypothesis of what processes and phenomena control sediment and wood dynamics and storage in small mountainous drainage basins. Simulation results presented here illuminate some aspects of interactions among these controls while raising new questions, some of which may be addressed by future field studies. For example, our results show a strong interaction between wood and sediment, and we have pointed out that burial of wood may slow its decay. By dating buried wood deposits we hope to quantify this effect.

6. CONCLUSIONS

The simulation indicates, and our field observations confirm, that wood and sediment dynamics are strongly linked. The coupling between sediment and wood implies a strong coupling between forests and channels. Through this coupling, forest conditions "drive" channel conditions, and forests, sediment dynamics, and channels are inextricably linked. Forest management practices that change forest conditions will inevitably change channel conditions and must therefore be carefully tailored to mitigate adverse impacts on riverine habitat.

Acknowledgements. This research was funded by the Coastal Landscape Analysis and Modeling Study (CLAMS), USDA Forest Service, Pacific Northwest Research Station. John Green, Simon Mudd, and Christine May assisted us in the field. Richard Iverson offered helpful advice concerning the debris flow runout model. Arjun Heimsath graciously shared his findings on soil production rates in the Oregon Coast Range. Michael Wimberly offered advice for modeling forest fires. Discussions with Lee Benda, Mauro Casadei, William Dietrich, Daniel Miller, David Montgomery, and Jonathan Stock yielded useful insight. Gregory Tucker, Nicole Gasparini, and Rafael Bras are continuing collaborators with the CHILD model and its offspring. Thorough reviews by William Dietrich, Faith Fitzpatrick, David Montgomery, and Gregory Tucker greatly improved the paper.

REFERENCES

Abbe, T.B., and D.R. Montgomery, Large woody debris jams, channel hydraulics and habitat formation in large rivers, *Reg. Rivers: Res. Mgmt.*, *12*, 201-221, 1996.

Benda, L.E., and T.W. Cundy, Predicting deposition of debris flows in mountain channels, *Can. Geotech. J.*, *27*(4), 409-417, 1990.

Benda, L., and T. Dunne, Stochastic forcing of sediment supply to channel networks from landsliding and debris flow, *Water Resour. Res., 33*(12), 2849-2863, 1997a.

Benda, L., and T. Dunne, Stochastic forcing of sediment routing and storage in channel networks, *Water Resour. Res., 33*(12), 2865-2880, 1997b.

Burroughs, E.R., Landslide hazard rating for portions of the Oregon Coast Range, in *Proceeding of Symposium on Effects of Forest Land Use on Erosion and Slope Stability*, pp. 265-274, East-West Cent., Univ. of Hawaii, Honolulu, 1984.

Burroughs, E.R., and B.R. Thomas, Declining root strength in Douglas fir after felling as a factor in slope stability, *Res. Pap. INT Intermt. For. Range Exp. Stn. INT-190*, 27 pp., 1977.

Dietrich, W.E., R. Reiss, M.-L. Hsu, and D.R. Montgomery, A process-based model for colluvial soil depth and shallow landsliding using digital elevation data, *Hydrol. Proc., 9*, 383-400, 1995.

Duan, J., *A Coupled Hydrologic-Geomorphic Model for Evaluating Effects of Vegetation Change on Watersheds*, Ph.D. Thesis,

133 pp., Oregon State Univ., Corvallis, 1996.

Duan, J., J. Selker, and G.E. Grant, Evaluation of probability density functions in precipitation models for the pacific northwest, *J. Am. Wat. Resour. Assoc., 34*(3), 617-627, 1998.

Eagleson, P.S., Climate, soil, and vegetation, 2, the distribution of annual precipitation derived from observed storm sequences, *Water Resour. Res., 14*(5), 713-721, 1978.

Engelund, F., and E. Hansen, *A Monograph on Sediment Transport in Alluvial Streams*, Teknisk Forlag, Copenhagen, 1972.

Flint, J.J., Stream gradient as a function of order, magnitude, and discharge, *Water Resour. Res., 10*, 969-973, 1974.

Garman, S.L., S.A. Acker, J.L. Ohmann, and T.A. Spies, Asymptotic height-diameter equations for twenty-four tree species in western Oregon, Forest Research Laboratory, Oregon State University, Corvallis, *Research Contribution 10*, 22 pp., 1995.

Govers, G., Evaluation of transporting capacity formulae for overland flow, in *Overland Flow*, ed. By A.J. Parsons and A.D. Abrahams, 243-273, Chapman & Hall, New York, 1992.

Hack, J.T., Studies of longitudinal stream profiles in Virginia and Maryland, *U.S. Geol. Surv. Prof. Pap., 294-B*, 1957.

Hammond, C., D. Hall, S. Miller, and P. Swetik, Level 1 stability analysis (LISA), documentation of version 2.0, *U.S. For. Ser. Gen. Tech. Rep. INT-285*, 190 pp., 1992.

Harmon, M.E., J.F. Franklin, F.J. Swanson, P. Sollins, S.V. Gregory, J.D. Lattin, N.H. Anderson, S.P. Cline, N.G. Aumen, J. Sedell, G.W. Lienkaemper, K. Cromack, Jr., and K.W. Cummins, Ecology of coarse woody debris in temperate ecosystems, *Adv. Ecol. Res., 15*, 133- 302, 1986.

Heimsath, A.M., W.E. Dietrich, K. Nishiizumi, and R.C. Finkel, The soil production function and landscape equilibrium, *Nature*, *388*, 358-361, 1997.

Heimsath, A.M., W.E. Dietrich, K. Nishiizumi, and R.C. Finkel, Stochastic processes of soil production and transport: erosion rates, topographic variation, and cosmogenic nuclides in the Oregon Coast Range, *Earth Surf. Processes Landforms*, in press, 2001.

Hogan, D.L., S.A. Bird, and M.A. Hassan, Spatial and temporal evolution of small coastal gravel- bed streams: Influence of forest management on channel morphology and fish habitats, in *Gravel-Bed Rivers in the Environment*, ed. by P.C., Klingeman, R.L. Beschta, P.D. Komar, and J.B. Bradley, pp. 365-392, Water Resources Publications, Highlands Ranch, CO, 1998.

Hough, B.K., *Basic Soils Engineering*, 513 pp., Ronald Press, New York, 1957.

Howard, A.D., and Kerby, G., Channel changes in badlands, *Geol. Soc. Amer. Bull., 94*, 739-752, 1983.

Huff, M.H., *Post-Fire Succession in the Olympic Mountains, Washington: Forest Vegetation, Fuels, and Avifauna*, Ph.D. dissertation, Univ. Washington, Seattle, 1984.

Ijjasz-Vasquez, E.J., and R.L. Bras, Scaling regimes of local slope versus contributing area in digital elevation models, *Geomorphology*, *12*(4), 299-311, 1995.

Iverson, R.M., The physics of debris flows, *Rev. Geophys., 35*(3), 245-296, 1997.

Iverson, R.M., Landslide triggering by rain infiltration, *Water Resour. Res., 36*(7), 1897-1910, 2000.

Iverson, R.M., M.E. Reid, and R.G. LaHusen, Debris-flow mobilization from landslides, *Annu. Rev. Earth Planet. Sci., 25*, 85-138, 1997.

Iverson, R.M., R.P. Denlinger, R.G. LaHusen, and M. Logan, Two-phase debris flow across 3-D terrain: model predictions and experimental tests, *Proceedings, Second International Conference on Debris-flow Hazards Mitigation*, Taiwan, 2000.

Kochel, R.C., D.F. Ritter, and J. Miller, Role of tree dams in the construction of pseudo-terraces and variable geomorphic responses to floods in Little River valley, Virginia, *Geology*, *15*, 718-721, 1987.

Lancaster, S.T., *A Nonlinear River Meandering Model and its Incorporation in a Landscape Evolution Model*, Ph.D. Thesis, 277 pp., Massachusetts Institute of Technology, Cambridge, 1998.

Leopold, L.B., and T. Maddock, Jr., The hydraulic geometry of stream channels and some physiographic implications, *U.S. Geol. Surv. Prof. Pap. 252*, 57 pp., 1953.

Lienkaemper, G.W., and F.J. Swanson, Dynamics of large woody debris in streams in old-growth Douglas-fir forests, *Can. J. For. Res.*, *17*, 150-156, 1987.

Lisle, T.E., J.M. Nelson, J. Pitlick, M.A. Madej, and B.L. Barkett, Variability of bed mobility in natural, gravel-bed channels and adjustments to sediment load at local and reach scales, *Water Resour. Res., 36*(12), 3743-3755, 2000.

Lisle, T.E., J.E. Pizzuto, H. Ikeda, F. Iseya, and Y. Kodama, Evolution of a sediment wave in an experimental channel, *Water Resour. Res., 33*(8), 1971-1981, 1997.

Long, C.J., C. Whitlock, P.J. Bartlein, and S.H. Millspaugh, A 9000-year fire history from the Oregon Coast Range, based on a high-resolution charcoal study, *Can. J. For. Res., 28*, 774-787, 1998.

Madej, M.A, and V. Ozaki, Channel response to sediment wave propagation and movement, Redwood Creek, California, USA, *Earth Surf. Processes Landform, 21*(10), 911-927, 1996.

Massong, T.M., and D.R. Montgomery, Influence of sediment supply, lithology, and wood debris on the distribution of bedrock and alluvial channels, *Geol. Soc. Amer. Bull.*, *112*(5), 591-599, 2000.

May, C.L., *Debris Flow Characteristics Associated with Forest Practices in the Central Oregon Coast Range*, M.S. Thesis, 121 pp., Oregon State Univ., Corvallis, 1998.

Means J.E., and T.E. Sabin, Height growth and site index curves for Douglas-fir in the Siuslaw National Forest, Oregon, *Western Journal of Applied Forestry, 4*(4), 136-142, 1989.

Moglen, G., and R.L. Bras, The effect of spatial heterogeneities on geomorphic expression in a model of basin evolution*, Water Resour. Res.*, 31(10), 2613-2623, 1995.

Montgomery, D.R., and W.E. Dietrich, Where do channels begin?, *Nature*, *336*, 232-234, 1988.

Montgomery, D.R., and W.E. Dietrich, Channel initiation and the problem of landscape scale, *Science*, *255*, 826-830, 1992.

Montgomery, D.R., and W.E. Dietrich, A physically based model for the topographic control on shallow landsliding, *Water*

Resour. Res., *30*(4), 1153-1171, 1994.

Montgomery, D.R., T.B. Abbe, J.M. Buffington, N.P. Peterson, K.M. Schmidt, and J.D. Stock, Distribution of bedrock and alluvial channel in forested mountain drainage basins, *Nature*, *318*, 587-589, 1996.

Montgomery, D.R., W.E. Dietrich, R. Torres, S.P. Anderson, J.T. Heffner, and K. Loague, Hydrologic response of a steep unchanneled valley to natural and applied rainfall, *Water Resour. Res.*, *33*, 91-109, 1997.

Montgomery, D.R., K.M. Schmidt, H.M. Greenberg, and W.E. Dietrich, Forest clearing and regional landsliding, *Geology*, *28*(4), 311-314, 2000.

Reeves, G.H., P.A. Bisson, and J.M. Dambacher, Fish communities, in *River Ecology and Management: Lessons from the Pacific Coastal Ecoregion*, ed. by R.J. Naiman and R.E. Bilby, pp. 200-234, Springer-Verlag, New York, 1998.

Reneau, S.L., W.E. Dietrich, M. Rubin, D.J. Donahue, and A.J.T. Jull, Analysis of hillslope erosion rates using dated colluvial deposits, *J. Geol.*, *97*, 47-63, 1989.

Reneau, S.L., and W.E. Dietrich, Erosion rates in the southern Oregon Coast Range: Evidence for an equilibrium between hillslope erosion and sediment yield, *Earth Surf. Processes Landforms*, *16*, 307-322, 1991.

Richards, F.J., A flexible growth function for empirical use, *J. Exp. Biol*., *10*, 290-300, 1959.

Robison, E.G., and R.L. Beschta, Identifying trees in riparian areas that can provide coarse woody debris to streams, *For. Sci.*, *36*(3), 790-801, 1990.

Robison, E.G., K. Mills, J. Paul, L. Dent, and A. Skaugset, Storm impacts and landslides of 1996: final report, *For. Pract. Tech. Rep. No. 4*, 145 pp., Oregon Department of Forestry, 1999.

Roering, J.J., J.W. Kirchner, and W.E. Dietrich, Evidence for nonlinear, diffusive sediment transport on hillslopes and implications for landscape morphology, *Water Resour. Res.*, *35*(3), 853-870, 1999.

Schmidt, K.M., J.J. Roering, J.D. Stock, W.E. Dietrich, and D.R. Montgomery, The variability of root cohesion as an influence on shallow landslide susceptibility in the Oregon Coast Range, *Can. Geotech. J.*, in press, 2001.

Schroeder, W.L., and J.V. Alto, Soil properties for slope stability analysis: Oregon and Washington Coastal Mountains, *For. Sci.*, *29*, 823-833, 1983.

Sidle, R.C., A conceptual model of changes in root cohesion in response to vegetation management, *J. Environ. Qual.*, *20*, 43-52, 1991.

Sidle, R.C., A theoretical model of the effects of timber harvesting on slope stability, *Water Resour. Res.*, *28*(7), 1897-1910, 1992.

Snyder, N.P., K.X Whipple, G.E. Tucker, and D.J. Merritts, Landscape response to tectonic forcing: Digital elevation model analysis of stream profiles in the Mendocino triple junction region, northern California. *Geol. Soc. Amer. Bull.*, *112*(8), 1250-1263, 2000.

Spies, T.A., J.F. Franklin, and T.B. Thomas, Coarse woody debris in Douglas-fir forests of western Oregon and Washington, *Ecology*, *69*(6), 1689-1702, 1988.

Swanson, F.J., M.M. Swanson, and C. Woods, *Inventory of mass erosion in the Mapleton Ranger District Siuslaw National Forest*, a cooperative study of the Siuslaw National Forest and the PNW Forest and Range Experiment Station, 1977.

Tarboton, D.G., R.L. Bras, and I. Rodriguez-Iturbe, On the extraction of channel networks from digital elevation data, *Hydrol. Processes*, *5*, 81-100, 1991.

Tucker, G.E., and R.L. Bras, Hillslope processes, drainage density, and landscape morphology, *Water Resour. Res.*, *34*, 2751-2764, 1998.

Tucker, G.E., and R.L. Bras, A Stochastic Approach to Modeling the Role of Rainfall Variability in Drainage Basin Evolution, *Water Resour. Res.*, *36*(7), 1953-1964, 2000.

Tucker, G.E., S.T. Lancaster, N.M. Gasparini, R.L. Bras, and S.M. Rybarczyk, An object-oriented framework for hydrologic and geomorphic modeling using triangulated irregular networks, *Comp. Geosci.*, in press, 2001a.

Tucker, G.E., S.T. Lancaster, N.M. Gasparini, and R.L. Bras, The channel-hillslope integrated landscape development (CHILD) model, *Landscape Erosion and Landscape Evolution Modeling*, GSA special volume, ed. by R.S. Harmon and W.W. Doe, III, in press, 2001b.

Van Sickle, J., and S.V. Gregory, Modeling inputs of large woody debris to streams from falling trees, *Can. J. For. Res.*, *20*(10), 1593-1601, 1990.

Vanoni, V.A., *Sedimentation Engineering*, A.S.C.E., New York, 1975.

Willgoose, G., A statistic for testing the elevation characteristics of landscape simulation models, *J. Geophys. Res.*, *99*(B7), 13,987-13,996, 1994.

Wimberly, M.C., T.A. Spies, C.J. Long, and C. Whitlock, Simulating historical variability in the amount of old forests in the Oregon Coast Range, *Conservation Biology*, *14*(1), 167-180, 2000.

Stephen T. Lancaster, Shannon K. Hayes and Gordon E. Grant, Forestry Sciences Laboratory, 3200 SW Jefferson Way, Corvallis, OR 97331